ACS APPLIED MATERIALS & INTERFACES

Research Article

www.acsami.org

Microscopic Investigations into the Effect of Surface Treatment of Cathode and Electron Transport Layer on the Performance of Inverted Organic Solar Cells

Shailendra Kumar Gupta,*[,†,‡] Rajeev Jindal,[‡] and Ashish Garg*[,†,‡]

[†]Department of Materials Science and Engineering and [‡]Samtel Center for Display Technologies, Indian Institute of Technology Kanpur, Kanpur 208016, India

ABSTRACT: Surface treatments of various layers in organic solar cells play a vital role in determining device characteristics. In this manuscript, we report on the influence of surface treatment of indium tin oxide (ITO) electrode and electron transport layer (ETL), ZnO, on the photovoltaic performance of inverted organic solar cells (IOSC) and their correlation with the surface chemistry and surface potential as studied using X-ray photoelectron spectroscopy (XPS) and Kelvin probe force microscopy (KPFM), using the device structure glass/ITO/ZnO/P3HT: PCBM/MoO_3/(Au or Ag) (P3HT, poly(3-hexylthiophene-2,5-diyl), and PCBM, phenyl-C61-butyric acid methyl ester). Our results show that although ozonization of ITO leads to an improvement in the device power conversion efficiency, the ozonization of a subsequent ZnO layer results in a decreased performance mainly because of a decrease in the fill factor (FF). However, subsequent methanol (CH_3OH) treatment of ZnO layer on an ozonized ITO electrode shows substantial improvement with device efficiencies exceeding ~4% along with superior reproducibility of the devices. Furthermore, a detailed analysis of the surface wettability, chemistry, and surface potential using contact angle measurements, XPS, and KPFM attribute the improvements to the elimination of surface defects and the changes in the surface potential. Finally, impedance analysis suggests that methanol treatment of the ZnO layers leads to the development of a favorable nanophase structure with higher conductivity, which is otherwise indiscernible using microscopic methods.

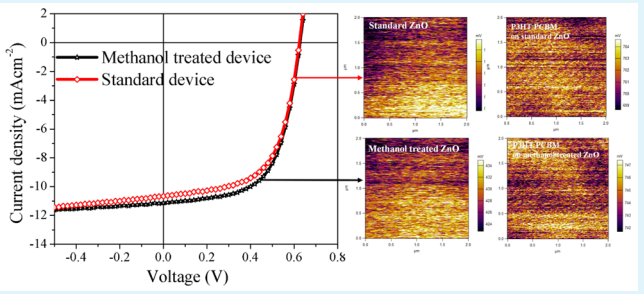

KEYWORDS: *inverted organic solar cells, surface treatment, P3HT:PCBM, X-ray photo spectroscopy, KPFM, solvent treatment*

INTRODUCTION

Organic solar cells (OSC) have been one of the most researched photovoltaic technologies over the past two decades or so, primarily because of their potential to become a low-cost photovoltaic technology driven by solution processability of the major constituents on rigid as well as flexible substrates.[1−3] The most commonly used device configuration is the bulk heterojunction (BHJ) type, where a blend of p-type semiconducting polymer (P3HT or poly(3-hexylthiophene-2,5-diyl), a workhorse material) and n-type material such as fullerene derivative (e.g., commonly used $PC_{60}BM$, phenyl-C61-butyric acid methyl ester) that is sandwiched between the anode and the cathode.[4,5] A typical device configuration for such a system is glass/ITO/PEDOT:PSS/P3HT:PCBM/Ca/Al where ITO (indium tin oxide) acts as anode for a collection of holes mediated by an intermediate hole transporting layer (HTL) of a PEDOT:PSS (poly(3,4-ethylenedioxythiophene) poly(styrene sulfonate)) layer, whereas Ca/Al are used as a top electrode for electron collection, acting as cathode. A major bottleneck of the devices fabricated in this configuration is their poor environmental stability, mainly attributed to the corrosiveness of PEDOT:PSS, which degrades the ITO electrode and the active layer.[6−9] This has led to the development of so-called inverted devices in which electrons flow to the ITO electrode, acting as cathode, and holes move toward the top of the device and get collected on a metal electrode, typically Ag or Au, acting as anode.[10] A typical configuration of such a device is glass/ITO/ZnO/P3HT:PCBM/HTL/metal (Ag).[11,12]

For these devices, ITO, a transparent conducting oxide, is typically used as the bottom electrode, because it has very little absorption in the visible region and possesses high electrical conductivity (sheet resistance ≈ 10 ohm cm^{-2}).[13−15] In OSC devices, as mentioned above, ITO can be used as either anode or cathode, depending on the type of device architecture driven by the use of carrier-selective buffer layer on it. For example, use of PEDOT:PSS on it makes it an anode for hole collection, whereas the use of ZnO on it makes it a cathode for electron collection.[16] It has been shown in various reports that the performance of an OSC device strongly depends on the morphology, effective work function, and carrier injection characteristics of the electrode.[17,18] Surface treatment of ITO is an important prerequisite because of the inherent presence of a subnanometer layer of nonconducting carbon contaminants as

Received: April 25, 2015
Accepted: July 9, 2015
Published: July 9, 2015

DOI: 10.1021/acsami.5b03583
ACS Appl. Mater. Interfaces 2015, 7, 16418−16427

explored by surface composition analysis,[19] which affect device performance adversely. In the literature, the importance of the ITO surface-modification procedure has been shown on polymer as well as small-molecule single-/bilayer organic devices, where active layers were directly deposited on to the ITO surface. For example, variations in device performance were seen because of differences in ITO surface treatments (methods and duration) with a dependence on driving voltage of organic light-emitting diode (OLED) devices.[15,20] Among these processes, prior to the deposition of next layer, the surface of ITO can be subjected to either one or a combination of any of the following: mechanical cleaning, plasma cleaning in different gas environments (oxygen, argon, or hydrogen), UV ozonization (UVO), wet cleaning (RCA, aqua regia), imposition of self-assemblies of monolayers, and heat treatment.[19,21−28] In all cases, surface characterization methods such as contact angle measurements coupled with spectroscopic methods such as Auger and X-ray photon spectroscopy (XPS), Hall measurements, and atomic force microscopy (AFM) show changes in various surface characteristics, e.g., surface chemical composition, charge carrier concentration, sheet resistance, work function, shift in the Fermi level, contact resistance, surface energy, and surface roughness values.[27,29]

As far as the effect of surface modification by UVO and air plasma on OSC devices is concerned, the removal of carbon atoms and increased O_2 concentration enhances the work function of ITO on glass as well as on PET substrates from 4.6 eV to 4.8−5.1 eV with treated ITO surface showing better electrical homogeneity because of a reduced charge-trap density.[30−32] Such changes lower the hole extraction barrier between P3HT and ITO and consequently enhance the short-circuit current density (J_{sc}) and fill factor (FF), as seen in normal OSC devices.[33] However, the effect has been found to be more pronounced in the absence of any HTL, and it leads to an improved device lifetime.[27,29] In inverted OSC architecture, the effect of moderate UVO treatment of dispersed ZnO−nanoparticle film results in improved J_{sc} and FF because of an improved wettability of the active layer on ZnO and hence better electronic coupling between ZnO and P3HT:PCBM as a result of the removal of organic surfactant.[34] Besides UVO treatment, solvent as well as monolayer treatment of ITO electrode have been shown to affect device performance, where dipoles at the surface play an important role in manipulating the vacuum level and morphology of the subsequent layer.[35,36] The role of UVO has also been criticized as unnecessary because preozonized solvent treatments are shown to be sufficient, although the latter could be substrate-dependent.[25] In the same way, polar solvent treatment of the constituent layers using methanol (CH_3OH) constituent layers in the OSC devices has been shown to be effective in improving device performance. In literature, methanol has been suggested to enhance the electrical conductivity and roughness of PEDOT:PSS films that in turn produce a favorable blend morphology.[37−40] In another study, methanol was used as a cleaning agent to remove surface residues from polymer blend, which helps to remove residues impurity/traps.[40]

However, despite the importance of these surface treatments, their exact role in determining device performance remains rather understudied, especially in terms of surface-related changes and consequent impacts on the energy band diagram. An understanding of the microscopic aspects of the surfaces upon surface treatments would help us determine appropriate surface treatment at each stage of the fabrication of devices having multilayered structures. Hence, in this manuscript we have investigated the effect of UVO treatment and solvent (methanol) treatment of the surface of the bottom electrode, i.e., ITO, and electron transport layer, i.e., ZnO, in an inverted OSC device with the structure glass/ITO (bottom)/ZnO/P3HT:PCBM/MoO_3/Au or Ag (top). The effects of these surface treatments on the characteristics of surface are investigated by transmittance and contact angle measurements as well as by Kelvin probe force microscopy (KPFM) and X-ray photoelectron spectroscopy (XPS). Our results suggest that whereas UVO treatment of ITO surface is beneficial to the device performance in all cases, the ZnO layer results in a superior device performance when it is methanol-treated versus when it is UVO-treated. This is attributed to changes in the surface wettability, surface potential, and the development of a favorable nanophase structure leading to device efficiencies exceeding 4%.

EXPERIMENTAL DETAILS

First, glass substrates coated with a 145 nm thin ITO layer (sheet resistance ≈ 10 ohm cm^{-2}) were ultrasonically cleaned in boiled soap solution for 15 min, followed by ultrasonication in DI water, acetone, and isopropyl alcohol (IPA) for 15 min, each followed by drying with nitrogen. Selected substrates were then exposed to the 10−15 min UVO treatment. Furthermore, 0.45 M ZnO solution was prepared by dissolving zinc acetate dihydrate in 2-methoxyethanol with monoethanolamine (MEA) used as stabilizer. ZnO thin films (30 nm) were grown by spin coating the solution on untreated as well as UVO-treated ITO substrates, followed by thermal drying at 250 °C for 10 min in air. Furthermore, although a few of the ZnO films were UVO treated (10 min), on a few of them methanol was spin coated at 1000 rpm in N_2 ambient immediately before the deposition of active-layer blend. Subsequently, 100 nm thin active layers were deposited by spin coating a P3HT:PCBM (1:1 w/w) blend solution, dissolved in chlorobenzene, followed by annealing on a hot plate at 150 °C in a nitrogen-filled glovebox. The samples were then transferred to a thermal evaporation chamber to deposit 10 nm thin layers of MoO_3 as HTL and 50 nm thin layer of Au or Ag as top electrode, both at 0.5 Å s^{-1}. The performance of unencapsulated devices of area 0.09 cm^2 was measured using a solar simulator under AM 1.5G illumination with intensity 100 mW cm^{-2}.

Thicknesses of all the thin films were measured using Bruker's DektakXT stylus profilometer. Optical transmission of the films was measured using PerkinElmer (LAMBDA-750) instrument, whereas contact angle measurements were carried out on Data Physics system. To get an insight into surface chemistry of the layers, XPS spectra were acquired using a PHI 5000 (Versa Prob II, FEI Inc.) spectrometer using a monochromatic Al Kα (1486.6 eV) source. Morphological and surface potential (KPFM) studies were conducted on Asylum MFP-3D AFM. Photovoltaic device characteristics were measured in dark as well as light (under 1 Sun/1.5G solar spectrum) using a Keithley 2600 source meter.

RESULTS AND DISCUSSION

To understand the effect of surface treatments on the optical and electrical characteristics of P3HT:PCBM, i.e., transmission and absorption behavior as well as device performance, we fabricated four different types of devices in the inverted configuration shown in Figure 1: (i) devices fabricated on ozonized ITO surface with subsequent ZnO buffer layer being unozonized, (ii) devices fabricated on ITO and ZnO, both without prior ozonization treatment, (iii) devices on ozonized ITO and ozonized ZnO (10 min), and (iv) devices on ozonized ITO but methanol-treated ZnO. The mechanism of ozonization has been depicted schematically in Figure 1. We first investigated the effect of these variations on the optical

DOI: 10.1021/acsami.5b03583
ACS Appl. Mater. Interfaces 2015, 7, 16418−16427

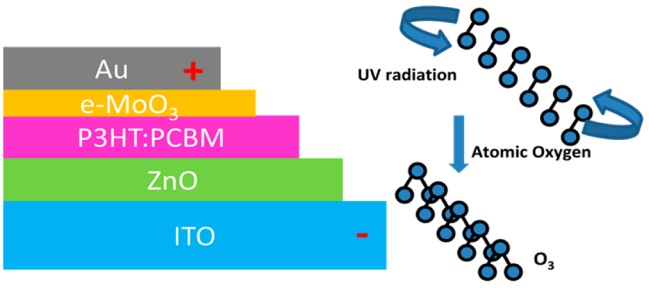

Figure 1. Schematic presentation of inverted device architecture and UV-ozonization process.

transmission characteristics of the ZnO/ITO structure and the absorption spectra of the subsequent active layer, i.e., P3HT:PCBM blend. As shown in Figure 2, we find no

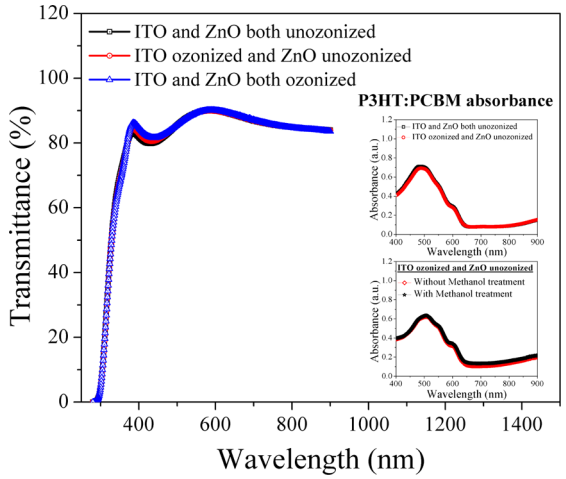

Figure 2. Transmittance spectra of ZnO/ITO bilayer under various conditions of UVO treatments. The inset shows the corresponding effect on the absorbance of P3HT:PCBM blend films.

appreciable change in the transmittance of ZnO/ITO (ZnO on ITO) structure, suggesting that UVO surface treatment of ITO and ZnO/ITO has no significant effect on the optical transmission characteristics. This is because the changes in the crystallite size in the film and surface roughness are not sufficient to warrant any surface scattering in all cases. Moreover, surface modification of ITO does not show any significant change in the absorbance of P3HT:PCBM films in the case of UV-assisted ozonization, whereas P3HT:PCBM films over methanol-treated ZnO show slightly improved absorbance, as shown in the inset of Figure 2. Also, in the case of latter, there is no change in the shape of the plots, ruling out any specific spectral enhancements. To ensure that slight enhancement in the absorbance of P3HT:PCBM films on methanol-treated ZnO is not due to changes in its thickness after methanol treatment of ZnO, we measured the thicknesses of two samples: one on untreated ZnO and another on methanol-treated ZnO. The measurements showed that the thickness of the active layer in both samples was 100 ± 3 nm, with the measurement accuracy of the stylus profilometer being ca. 1 nm. However, because the increase in the absorbance is only marginal, it is most likely due to subtle changes in the nanoscale morphology of the films, which are discussed in subsequent sections.

We further probed the surface wetting characteristics of these layers following UVO treatment of ITO and ZnO as well as methanol treatment of the ZnO grown on treated as well as untreated ITO surface by making contact angle measurements. As depicted in Figure 3, nonozonized ITO surface shows a contact angle of 28.3° (Figure 3a), whereas the UVO-treated ITO surface shows a contact angle of 17.8° (Figure 3b), leading to improved hydrophilicity of ITO surface. This is believed to be due to removal of various surface organic contaminants caused by UVO treatment of the surface, which enhances the surface energy of ITO/air interface (γ_{sg}) in comparison to the surface energy of ITO/liquid interface (γ_{sl}), causing a reduction in the contact angle and consequently leading to an improvement in the wettability of the ITO surface for spin coating of a subsequent ZnO layer using a liquid precursor. Moreover, the change in the contact angle of ITO surface by UVO treatment is manifested by the slight change in the roughness of subsequent ZnO layer as suggested by atomic force microscopy images (not shown) and the contact angle on the surface of ZnO film. The contact angle of liquid droplets on ZnO surface that was grown on UVO-treated ITO is smaller (30.9°) than that on ZnO film grown over unozonized ITO (36.3°), suggesting that a UVO-treated ITO surface leads to a ZnO surface with slightly higher hydrophilicity. The contact angle on ZnO surface also goes down to 17.1° once the ZnO surface is UVO treated for 10 min. However, the literature suggests that the mixture of P3HT:PCBM dissolved in chrolorobenzene has high surface tension; hence, it is expected that a relatively more hydrophobic surface will lead to conducive growth of P3HT:PCBM film resulting in a favorable microstructure in the film and consequently improved device performance.[41,42] To examine the role of hydrophobicity of the ZnO surface on the subsequent active-layer morphology, we further treated the ZnO surface by spin coating methanol (CH_3OH) over thermally dried but untreated ZnO surface grown on ozonized ITO. The contact angle measurement shows a value of ~38.8°, which is larger than the values obtained on both untreated as well as UVO-treated ZnO surfaces (30.9 and 17.1°, respectively), all grown on ozonized ITO, hence suggesting an increase in the hydrophobicity of the ZnO surface upon methanol treatment.

Then, we looked at the effect of these surface treatment variations on the performance of OSC devices, and Figure 4a,b shows the current density ($J-V$) curves of the devices fabricated on these ZnO and ITO layers with different combinations of UVO surface treatments. Although all the curves show good dark and light characteristics, the difference between various device parameters, i.e., J_{sc}, open-circuit voltage (V_{OC}), and FF as summarized in Table 1, suggest an improvement in J_{sc} for the devices fabricated on ozonized ITO over unozonized ITO with ZnO remaining unozonized in both cases, in agreement with the results achieved in normal OSC devices.[30] Because V_{OC} depends on the energy level differences between the constituents (P3HT and PCBM) of the active-layer blend, it should remain independent of the surface modification, as clearly seen here. The slightly lower series resistance (R_S) but enhanced shunt resistance (R_{SH}) for the device on ozonized ITO ($R_S \approx 11.0\ \Omega\ cm^{-2}$ and $R_{SH} \approx 1210\ \Omega\ cm^{-2}$) may be attributed to the removal of unwanted C atoms adsorbed onto ITO under UVO exposure, leading to reduced interfacial trap density and consequently reduced leakage. In contrast, the effect of a 10 min UVO treatment of the ZnO layer on an ozonized ITO layer shows a marked reduction in

DOI: 10.1021/acsami.5b03583
ACS Appl. Mater. Interfaces 2015, 7, 16418−16427

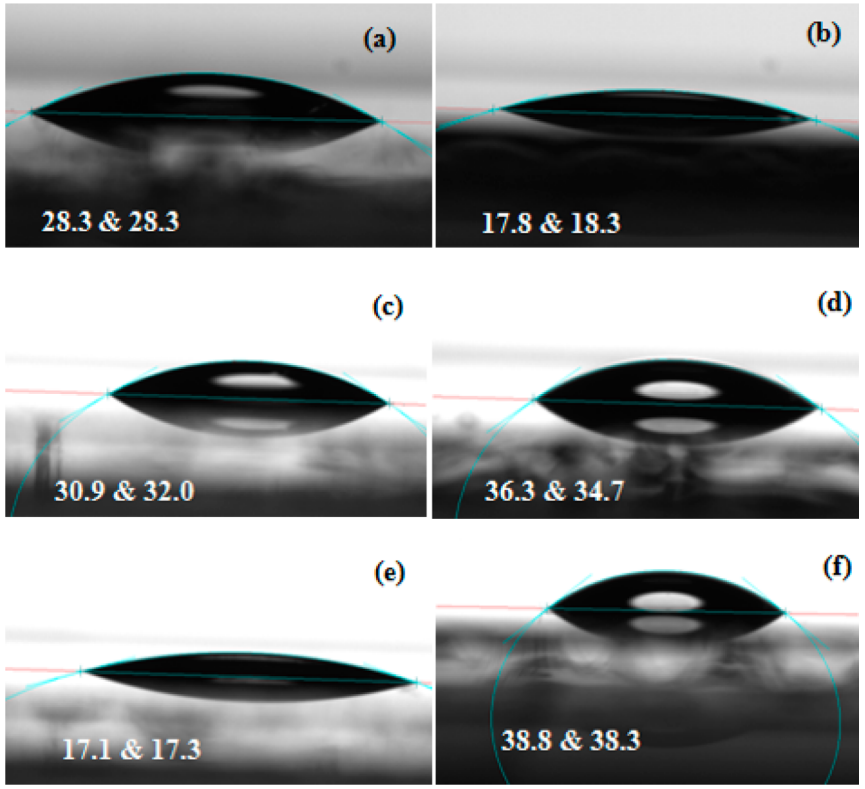

Figure 3. Contact angle measurements over (a) untreated ITO, (b) UVO-treated ITO, (c) untreated ZnO surface on UVO-treated ITO, (d) untreated ZnO on untreated ITO, (e) UVO-treated ZnO on UVO-treated ITO, and (f) methanol-treated ZnO on UVO-treated ITO.

both J_{sc} and FF, which is aided mainly by enhanced R_S (27 Ω cm^{-2}) and much reduced R_{SH} (365 Ω cm^{-2}), leading to larger leakage and hence higher reduction in the charge extraction efficiency and a reduced fill factor.

We correlate these data with the results of contact angle measurements shown in Figure 3. The comparison shows that the unozonized ZnO on ITO shows a more hydrophobic surface compared to UVO-treated ZnO largely because of the removal of carbon atoms from the ZnO surface, possibly leading to poor P3HT:PCBM film quality for UVO-treated ITO/ZnO. In contrast, excessive UVO treatment for 10 min leads to an increase in adsorbed oxygen (O_2) defects over the ITO/ZnO surface, which increases Zn−O bond density. Such effects may disrupt the interfacial band alignment between ITO/ZnO and polymer interface in a way that decreases the charge extraction efficiency because of charge build up inside the blend. The schematic picture of such misalignment at the interface between ozonized ZnO and PCBM is shown in Figure 5a−c. Ozonized ZnO has been shown to possess a higher work function because of oxygen defects in comparison to that of unozonized ZnO surface[43], which is also confirmed by the XPS spectroscopy results shown in Figure 6 and is discussed later. Under these modified band level conditions, relative positions of energy level of ZnO will also change with respect to PCBM. In thermal equilibrium, once PCBM and ZnO work functions are matched, a barrier to carrier movement (in both injection as well as extraction) is created in the case of ozonized ZnO (Figure 5c) in comparison to unozonized ZnO surface (Figure 5b). This appears to be appropriate because whereas ZnO growth requires a hydrophilic surface as a result of the hydrated nature of its precursors, P3HT:PCBM blend requires a hydrophobic surface because of the hydrophobic nonpolar solvent, i.e., chlorobenzene. The change in dark current with surface treatment suggests the effect on the injection characteristics of the electrodes, as shown in Figure 4b (10 min). UV illumination of the ZnO layer leads to photoinduced shunt paths in the films, possibly because of the creation of interfacial defects or change in the band alignment at the ZnO and polymer interface. Similar observations of change in band alignment under fluorination and light-soaking processes of TiO_x were made in inverted organic solar cells.[44] Overall, it is interesting to note that ITO ozonization prior to ZnO fabrication results in a better device whereas ZnO ozonization prior to P3HT:PCBM growth results in an inferior device performance.

In Figure 4c,d, we demonstrate the performance of the devices fabricated using methanol-treated ZnO films grown on ozonized ITO/glass substrates. As shown in the Figure 4c,d and Table 2, the devices on methanol-treated ZnO layers show improved PCE by about 10% aided mainly by an increase in J_{sc}, as compared to that of the standard device (device fabricated on untreated ZnO and ozonized ITO). These results clearly highlight the beneficial role of methanol treatment in improving device performance and are corroborated by various other reports using methanol treatment of various layers, including that of the active layer.[45,46] Although qualitatively these changes are attributed to changes in the microstructure and energy band landscape, there is a need to understand the microscopic reasons behind these changes, which are further investigated in subsequent sections using surface characterization methods, namely, XPS and KPFM.

To gain a further understanding of how surface treatments affect device performance, we carried out XPS of various layers. We first analyzed the effect of UVO treatment on untreated and

DOI: 10.1021/acsami.5b03583
ACS Appl. Mater. Interfaces 2015, 7, 16418−16427

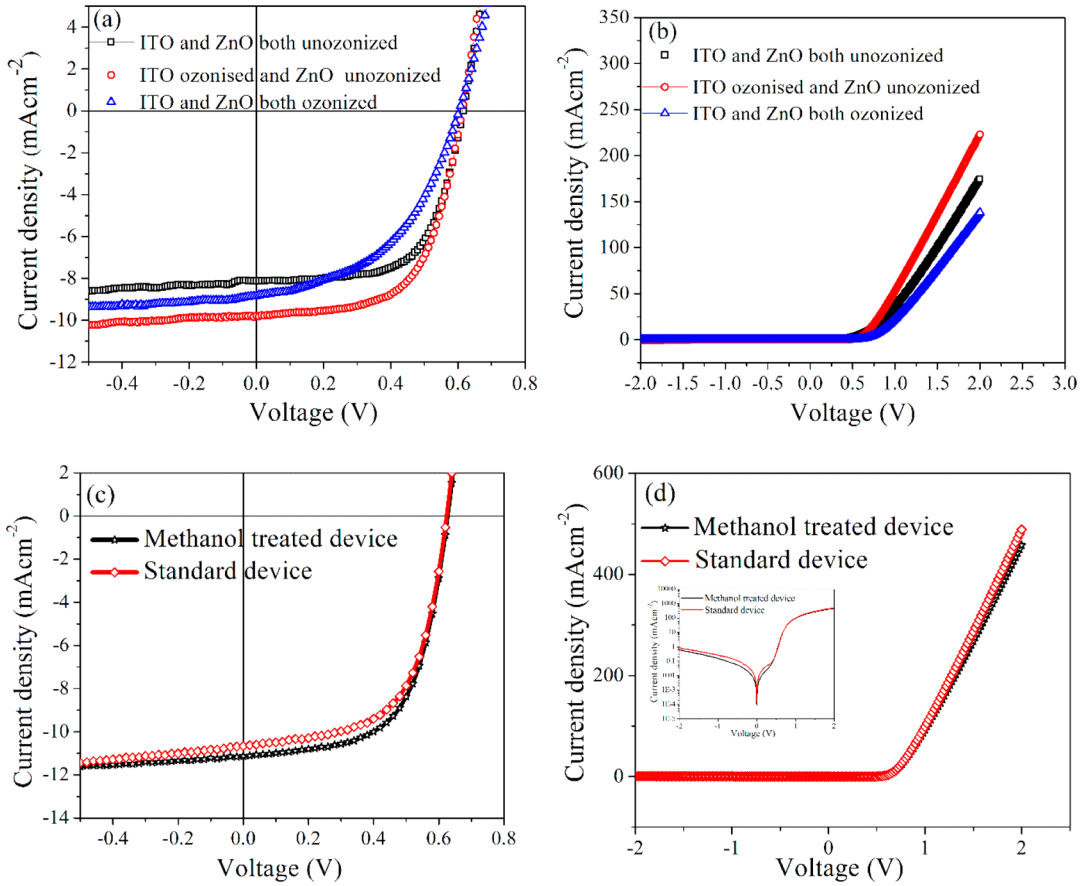

Figure 4. (a) Light and (b) dark current density (J) vs voltage (V) characteristics of inverted OSC devices with device structure glass/ITO/ZnO (30 nm)/P3HT: PCBM (100 nm)/MoO_3 (5 nm)/Ag (50 nm), with different combinations of surface treatments of ZnO and ITO layers. (c) Light and (d) dark $J-V$ characteristics of inverted OSC devices, with device structure glass/ITO/ZnO (30 nm)/P3HT: PCBM (100 nm)/MoO_3 (5 nm)/Ag (50 nm) with and without methanol treatment of ZnO layer.

Table 1. Device Parameters Measured at 1 Sun Illumination of Inverted OSC Devices Vis-à-Vis Surface Treatment of ITO Electrode and 30 nm Thin ZnO Electron Transport Layer[a]

device	J_{sc} (mA cm^{-2})	V_{oc} (V)	FF	η (%)	R_S (Ω cm^{-2})	R_{SH} (Ω cm^{-2})
ITO and ZnO both un ozonized	8.23 ± 0.17	0.61 ± 0.003	0.61 ± 0.023	3.14 ± 0.10	12.6 ± 0.6	849 ± 185
ITO ozonized and ZnO un ozonized	9.46 ± 0.27	0.61 ± 0.003	0.60 ± 0.015	3.45 ± 0.20	11.1 ± 0.12	1210 ± 417
ITO and ZnO both ozonized	8.68 ± 0.24	0.60	0.44 ± 0.030	2.29 ± 0.17	27 ± 2.9	365 ± 58

[a] J_{sc}: short circuit current density, V_{oc}: open circuit voltage, FF: fill factor, η: power conversion efficiency, R_s: series resistance, and R_{sh}: shunt resistance.

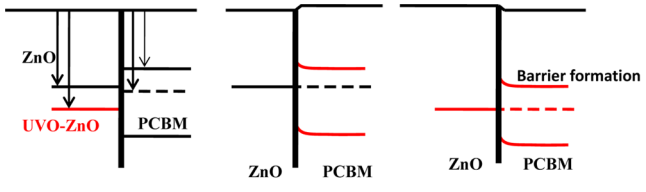

Figure 5. Schematic energy band diagram of the ZnO/PCBM interface (a) before contact and in thermal equilibrium, (b) with unozonized ZnO, and (c) with UVO-treated ZnO.

UVO-treated ZnO surfaces, and the results are shown in Figure 6a–c, comparing the concentration and peak binding energy changes in the peak profiles of C,O, and Zn atoms. First, we observe that the C 1s peak becomes substantially weaker after UVO treatment of ZnO, indicating the removal of C from the UVO-treated ZnO film and thus increasing the hydrophilicity of ZnO surface because of lower C concentration. It is plausible that the loss of adsorbed C in UVO-treated ZnO enhances the work function of ZnO surface because of a upward shift of vacuum level, as depicted in Figure 5b,c. We further deconvoluted C 1s peaks by fitting with Lorentzian–Gaussian, and the peaks were identified separately as C–H or C–C, C–O and C═O, or COO^- at 283.65, 285.50, and 287.73 eV, respectively. The results suggest that after UVO treatment C–C and C–O peaks shift to lower binding energies whereas C═O and COO– peaks shift to higher binding energies. Furthermore, the XPS spectra for O 1s peaks depicts a wide and asymmetric peak that was further deconvoulted into two peaks centered at different binding energies indicating the presence of different O species. The peak centered at lower binding energy shows the presence of O^{2-} in ZnO lattice, whereas that at higher binding energy represents deficient O^{2-}/–OH/loosely attached O inherently present in the film. The

DOI: 10.1021/acsami.5b03583
ACS Appl. Mater. Interfaces 2015, 7, 16418–16427

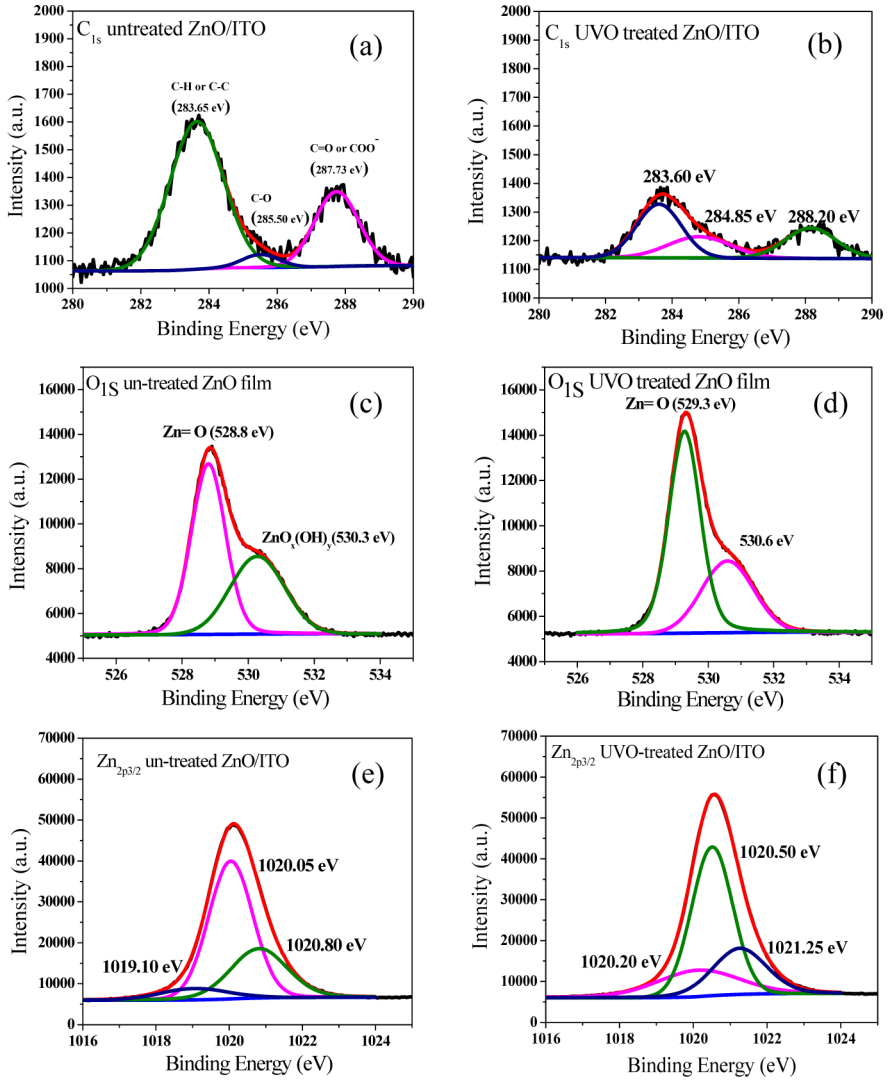

Figure 6. XPS spectra of UVO-treated and untreated, respectively, ZnO thin films showing the peaks for (a and b) C 1s, (c and d) O 1s, and (e and f) Zn 2p.

Table 2. Device Parameters of OSC Devices With and Without Methanol Treatment of ZnO (ZnO: 30 nm, P3HT:PCBM (1:0.8 wt %): 100 nm, MoO_3: 10 nm and Ag: 50 nm) Measured at 1 Sun Illumination

device	J_{sc} (mA cm^{-2})	V_{oc} (V)	FF	η (%)	R_S	R_{SH}
untreated ZnO (standard)	10.45 ± 0.43	0.62	0.585 ± 0.02	3.71 ± 0.16	8.5 ± 0.36	723 ± 58
methanol-treated ZnO	11.27 ± 0.4	0.62	0.594 ± 0.02	4.14 ± 0.12	7.8 ± 0.18	826 ± 128

difference between the two lies in the intensities and the position of two peaks when we consider untreated and UVO-treated ZnO films. UVO-treated film shows peak shifting toward higher binding energies and a decrease in the intensity of O deficiency, suggesting a decreased O vacancy concentration that may cause a downward shift of Fermi level or enhanced work function (Figure 6b,c) leading to a band misalignment at the ZnO/PCBM interfaces as also depicted in Figure 5c earlier. In a similar manner, the Zn $2p_{3/2}$ core line for both the cases shows a central deconvoluted peak shifted toward higher binding energy from 1020.05 to 1020.50 eV when treated with UVO. It signifies that 10 min UVO treatment leads to an increase in the adsorbed oxygen (O_2) defects over ZnO/ITO surface, which increases the number of Zn−O bonds and results in an increased oxidation of Zn; thus, the peak for UVO-treated ZnO layer shifts toward higher binding energy by ∼0.45 eV. This is possibly due to an increase in the concentration of surrounding electronegative O atoms after UVO treatment that further oppose the exclusion of electrons from the Zn atom. Such a shift should also be present in the determination of ZnO surface work function and possibly increases the barrier between ZnO and PCBM to inject/extract the charge carriers and decrease the FF, attributed to the disruption of the interfacial band alignment between ZnO and polymer interface in a way that decreases the extraction efficiency (Figure 5).

To understand further the role of methanol treatment over ZnO surface and consequently on the P3HT:PCBM blend, we carried out KPFM imaging and measurements as shown in Figure 7. KPFM is an AFM-based technique that is used to determine the work functions and potential at the surfaces.[47]

DOI: 10.1021/acsami.5b03583
ACS Appl. Mater. Interfaces 2015, 7, 16418−16427

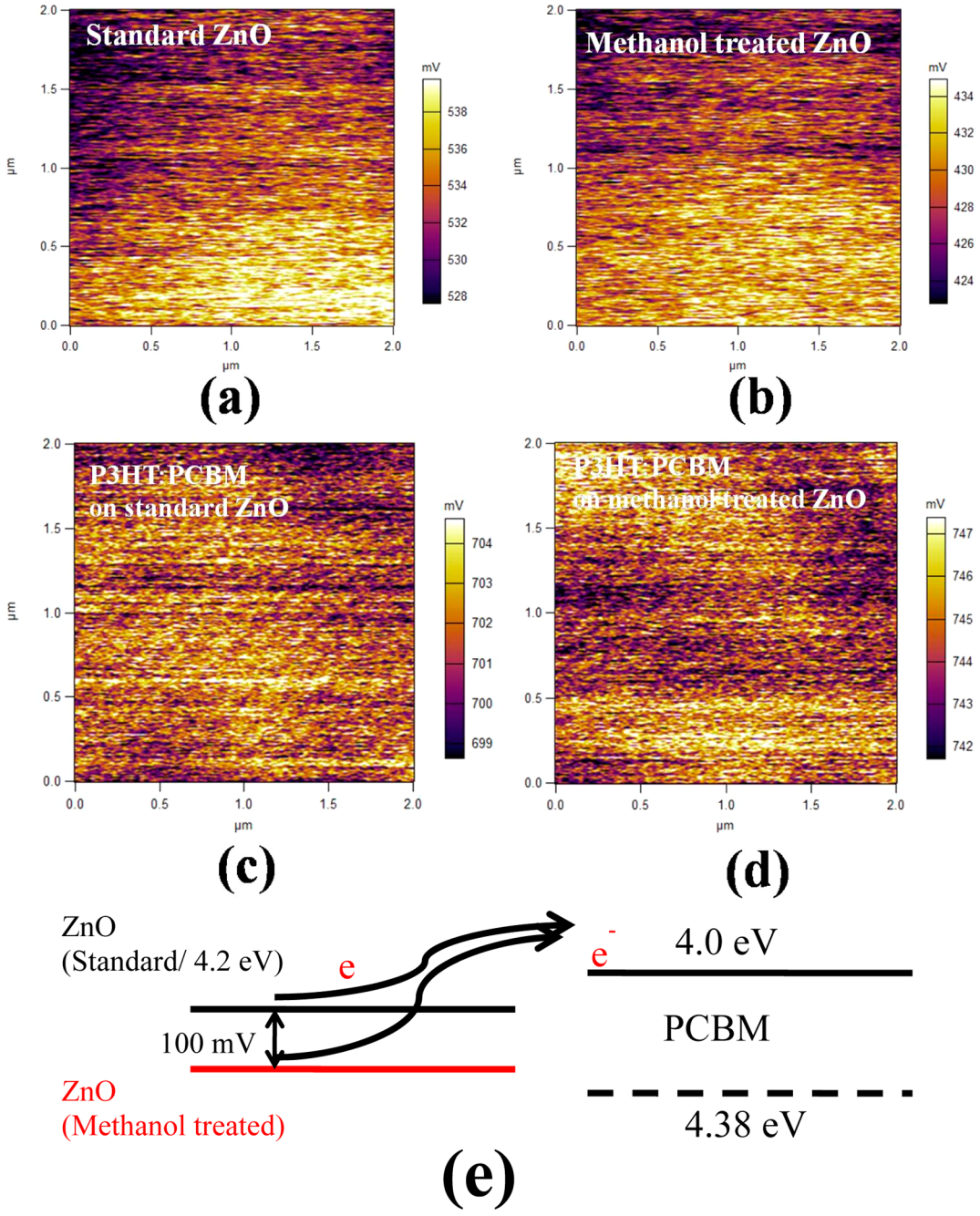

Figure 7. KPFM images of ZnO films (a) without and (b) with methanol treatment and P3HT:PCBM films grown on ZnO layer (c) without and (d) with methanol treatment showing surface potential maps, and (e) schematic representation of ZnO/PCBM interface.

The distributed contact potential difference (CPD) between the tip and the sample is calculated using eq 1.

$$V_{CPD} = \frac{\phi_{tip} - \phi_{sample}}{-e} \quad (1)$$

where e is the electronic charge and ϕ_{tip} (~5.0 eV) and ϕ_{sample} are the work functions of the tip and the sample, respectively. Here, ϕ_{tip} has a higher work function and a negative external voltage has been employed to the sample to nullify V_{CPD}. The scan area was 2 μm × 2 μm. As the results in Figure 7a,b suggest, the methanol-treated ZnO film (424−434 mV) shows an ca. 100 mV decrease in the surface potential compared to that of standard ZnO films (528−538 mV), suggesting that the work function of ZnO surface increases because of methanol treatment. This could be because the adsorbed O on the ZnO surface reacts with methanol molecules leading to a reduction in their concentration, signifying the role of methanol as a cleaning agent for ZnO surface. In a similar manner, as shown in Figure 7c,d, the surface potential measured for P3HT:PCBM films grown over methanol-treated ZnO shows a 50 mV increase in the surface potential because of the removal of surface traps resulting from a cosolvent effect, triggered by two simultaneous processes: methanol evaporation and thermal drying of the active layer. This shift in surface potential results in an improved electrical performance as we see from Figure 4c,d and is also corroborated by the literature.[37] The schematic diagram of energy levels in Figure 4e shows the enhanced work function for methanol-treated ZnO that will not contribute to

DOI: 10.1021/acsami.5b03583
ACS Appl. Mater. Interfaces 2015, 7, 16418−16427

the barrier during charge extraction as shown earlier in case of ozonized ZnO (Figure 5); however, the 100 mV downward shift in the Fermi level introduces an additional barrier to the electron's flow to PCBM in the dark, which leads to slight decrease in the forward current as shown in inset Figure 4d.

We further examined the surface morphology of ZnO and P3HT:PCBM films before and after methanol treatment using AFM and found that the morphology remains nearly the same with a slight decrease in the roughness of methanol-treated ZnO to 4.85 nm, down from 5.40 nm for untreated films. However, P3HT:PCBM film roughness values remain nearly the same. This marginal change in the roughness of ZnO after methanol treatment may be one of the factors behind slightly improved absorbance of active layer as observed in the inset of Figure 2.

However, similar to any other surface treatment such as oxygen plasma or UVO treatments, methanol treatment is also likely to be effective only if the active layer is deposited immediately after the methanol treatment of ZnO. Interestingly, in our studies, KPFM measurements of both ZnO and the active layer were carried out for a significant length of time by taking the samples out of the glovebox in the ambient, and the measurements remained consistent with time because the difference observed between the treated and untreated samples remains nearly the same. The active layer, however, is annealed soon after the deposition. Hence, methanol, being a low boiling point (60 °C) solvent, is likely to start evaporating before chlorobenzene (boiling point: 130 °C) during annealing. However, it is possible that because methanol evaporates through the active layer its effect may be quite similar to the effect of solvent treatment where devices are annealed in the presence of solvent vapor.[48] In our case, the potential measurements suggest that methanol also leads to an increase in the work function of ZnO, which is suggestive of an effect akin to surface cleaning. Hence, in our samples the role of methanol in improving the device appears to be twofold: (i) cleaning the ZnO surface and (ii) improving the morphology of the active layer by coevaporating.

To understand the changes in device characteristics with and without methanol treatment of the ZnO surface, we conducted frequency-dependent impedance analysis of the devices. Figure 8 shows the frequency-dependent plots of real (Z′) versus imaginary (Z″) parts of impedance, also called as Cole−Cole plots, measured at an excitation voltage of 0.5 V. Although an ideal Debye type behavior is represented by semicircles, our samples show two overlapping semicircles, manifesting the interface (left) and bulk (right) contributions. The plots are distinguished by high- and low-frequency regions signifying the transport (resistance, characteristic diffusion time, and global mobility) and recombination of minority charges (effective lifetime and recombination resistance) properties, respectively. On the basis of these observations, the equivalent circuit of the device is represented by a pair of RC networks for equivalent circuit fitted by using an EIS spectrum analyzer.[49−53]

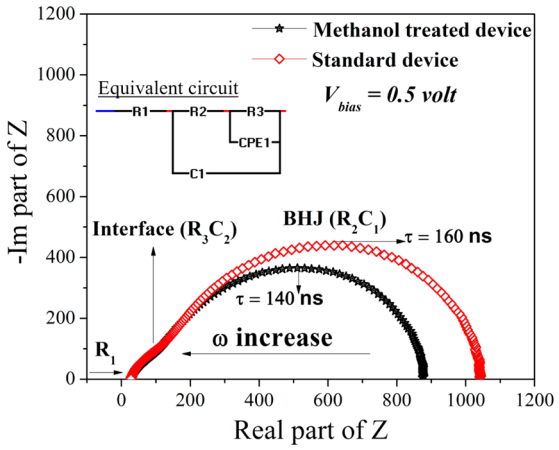

Figure 8. Cole−Cole plots of P3HT:PCBM devices fabricated on methanol-treated and untreated ZnO ETL layers. The inset shows the fitting with equivalent circuit having two R−C elements.

Here, we see that the difference between the two samples is primarily in the high-frequency semicircle (R_2C_1) belonging to the device interfaces, and the low-frequency semicircle, represented by R_3, CPE, defines the bulk heterojunction itself, where $R_2$and R_3 are defined as transport and recombination resistances, respectively, and C_1 and CPE are defined as capacitances corresponding to the depletion and chemical capacitance in the device, respectively. The reduced radius of the low-frequency semicircle in the presence of a methanol-treated ZnO layer suggests decreased impedances of the device compared to that of a standard OSC device implying higher conductivity of P3HT:PCBM blend in methanol-treated devices. Also, the leftward shift in the peak frequency at $\omega\tau$ = 1 suggests lower time constant (lifetime) in the methanol-treated devices.[54] The measured lifetime (τ) is voltage-dependent because the diameter of the low-frequency semicircle strictly depends on the bias voltage as it decreases with increasing voltage (V_{bias}); hence, τ decreases with increasing voltage as manifested by the shift of the peak frequency toward higher frequency, $\omega\tau$ = 1. The values of τ calculated from the peak frequency in Cole−Cole plot for P3HT:PCBM devices without and with methanol treatment are 160 and 140 ns, respectively. This time constant relates to carrier recombination lifetime and is determined by the nature of distributed interfaces between P3HT and PCBM in the bulk of active-layer blend and hence interaction between two phases. Reduction of recombination lifetime (τ) with methanol treatment suggests interfacial changes leading to reduced interfacial resistance between P3HT and PCBM. Such reduced interfacial resistance will assist in enhancing exciton-dissociating capability under illumination, thus leading to improved charge transport and J_{sc}. This is attributed to the nanoscale changes in morphology, which are otherwise indiscernible using microscopic methods, in particular the changes taking place perpendicular to the substrate. It is plausible that the soaking effect of methanol in the P3HT:PCBM blend and its subsequent evaporation may affect the growth of morphological constituents preferably in the vertical direction, thus enhancing the charge transport as observed in a few studies.[55,56]

The inverted OSC device architecture employed in the present work comprises ZnO and MoO_3 as carrier-selective layers. The estimated injection barriers are low in these devices: 0.2 eV at the ZnO/PCBM interface and 0.1 eV at the P3HT/MoO_3 interface, implying that both buffer layers make good ohmic contacts (Φ < 0.3 eV) with the active layer blend (P3HT:PCBM). This implies that both the electrodes are capable of injecting the carriers and that diffusion of both electrons and holes would be expected in the active layer. Hence, the lifetime (τ) we obtain would be an effective value of both the carriers, which is also suggested in the previous work.[49]

DOI: 10.1021/acsami.5b03583
ACS Appl. Mater. Interfaces 2015, 7, 16418−16427

CONCLUSIONS

We have correlated the effect of various surface treatments on the performance of inverted organic solar cell devices (Ag/MoO_3/P3HT:PCBM/ZnO/ITO/glass) with the changes in the surface chemistry as well as surface potential observed using XPS and KPFM. Our results suggest that UVO treatment of ITO electrode is beneficial in improving device performance whereas UVO treatment of ZnO (the electron transport layer) does not improve device performance. Rather, it is the methanol treatment of the ZnO surface that leads to an improved performance of the device, leading to device efficiencies well over 4%. The detailed investigations using XPS and KPFM show that this happens because of the changes in the surface chemistry associated with the defects on the surface of ZnO upon UVO treatment resulting in a change in the surface potential or work function of ZnO surface. UVO treatment of the ZnO surface leads to a reduction in carbonaceous matter on the surface and increased concentration of oxygen species on ZnO, giving rise to change in the work function of ZnO and leading to the formation an energy barrier to the flow of carriers from the blend. In addition, further methanol treatment of untreated ZnO leads to further improvement in device performance attributable to changes in the surface potential, as shown by KPFM, as well as nanoscale morphological changes in the active layer, as suggested by impedance analysis, which are indiscernible in AFM.

AUTHOR INFORMATION

Corresponding Authors

*Fax: +91-512-259-7505. E-mail: guptsk@iitk.ac.in.

*E-mail: ashishg@iitk.ac.in.

Notes

The authors declare no competing financial interest.

ACKNOWLEDGMENTS

We thank the Department of Science and Technology (DST) for funding through India-UK project APEX and Department of Electronics and Information Technology for financial support via National Centre on Flexible Electronics.

REFERENCES

(1) Nickel, F.; Haas, T.; Wegner, E.; Bahro, D.; Salehin, S.; Kraft, O.; A. Gruber, P.; Colsmann, A. Mechanically Robust, ITO-Free, 4.8% Efficient, All-Solution Processed Organic Solar Cells on Flexible PET Foil. *Sol. Energy Mater. Sol. Cells* **2014**, *130* (0), 317−321.

(2) Kang, S.-B.; Noh, Y.-J.; Na, S.-I.; Kim, H.-K. Brush-Painted Flexible Organic Solar Cells Using Highly Transparent and Flexible Ag Nanowire Network Electrodes. *Sol. Energy Mater. Sol. Cells* **2014**, *122* (0), 152−157.

(3) Choi, K.-H.; Kim, J.; Noh, Y.-J.; Na, S.-I.; Kim, H.-K. Ag Nanowire-Embedded ITO Films as a near-Infrared Transparent and Flexible Anode for Flexible Organic Solar Cells. *Sol. Energy Mater. Sol. Cells* **2013**, *110* (0), 147−153.

(4) Yu, G.; Gao, J.; Hummelen, J. C.; Wudl, F.; Heeger, A. J. Polymer Photovoltaic Cells: Enhanced Efficiencies Via a Network of Internal Donor-Acceptor Heterojunctions. *Science* **1995**, *270* (5243), 1789−1791.

(5) Halls, J. J. M.; Walsh, C. A.; Greenham, N. C.; Marseglia, E. A.; Friend, R. H.; Moratti, S. C.; Holmes, A. B. Efficient Photodiodes from Interpenetrating Polymer Networks. *Nature* **1995**, *376* (6540), 498−500.

(6) Girtan, M.; Rusu, M. Role of ITO and PEDOT:PSS in Stability/Degradation of Polymer:Fullerene Bulk Heterojunctions Solar Cells. *Sol. Energy Mater. Sol. Cells* **2010**, *94* (3), 446−450.

(7) Kawano, K.; Pacios, R.; Poplavskyy, D.; Nelson, J.; Bradley, D. D. C.; Durrant, J. R. Degradation of Organic Solar Cells Due to Air Exposure. *Sol. Energy Mater. Sol. Cells* **2006**, *90* (20), 3520−3530.

(8) de Jong, M. P.; van Ijzendoorn, L. J.; de Voigt, M. J. A. Stability of the Interface between Indium-Tin-Oxide and Poly(3,4-Ethylenedioxythiophene)/Poly(Styrenesulfonate) in Polymer Light-Emitting Diodes. *Appl. Phys. Lett.* **2000**, *77* (14), 2255.

(9) Garg, A.; Gupta, S. K.; Jasieniak, J. J.; Singh, T. B.; Watkins, S. E. Improved Lifetimes of Organic Solar Cells with Solution-Processed Molybdenum Oxide Anode-Modifying Layers. *Prog. Photovoltaics* **2015**, *23*, 989.

(10) Hau, S. K.; Yip, H.-L.; Baek, N. S.; Zou, J.; O'Malley, K.; Jen, A. K.-Y. Air-Stable Inverted Flexible Polymer Solar Cells Using Zinc Oxide Nanoparticles as an Electron Selective Layer. *Appl. Phys. Lett.* **2008**, *92* (25), 253301.

(11) Noh, Y.-J.; Na, S.-I.; Kim, S.-S. Inverted Polymer Solar Cells Including ZnO Electron Transport Layer Fabricated by Facile Spray Pyrolysis. *Sol. Energy Mater. Sol. Cells* **2013**, *117* (0), 139−144.

(12) Kyaw, A. K. K.; Sun, X. W.; Jiang, C. Y.; Lo, G. Q.; Zhao, D. W.; Kwong, D. L. An Inverted Organic Solar Cell Employing a Sol-Gel Derived ZnO Electron Selective Layer and Thermal Evaporated MoO3 Hole Selective Layer. *Appl. Phys. Lett.* **2008**, *93* (22), 221107.

(13) Wu, C. C.; Wu, C. I.; Sturm, J. C.; Kahn, A. Surface Modification of Indium Tin Oxide by Plasma Treatment: An Effective Method to Improve the Efficiency, Brightness, and Reliability of Organic Light Emitting Devices. *Appl. Phys. Lett.* **1997**, *70* (11), 1348−1350.

(14) Stadler, A. Transparent Conducting Oxides—an up-to-Date Overview. *Materials* **2012**, *5* (4), 661−683.

(15) Osada, T.; Kugler, T.; Bröms, P.; Salaneck, W. R. Polymer-Based Light-Emitting Devices: Investigations on the Role of the Indium—Tin Oxide (ITO) Electrode. *Synth. Met.* **1998**, *96* (1), 77−80.

(16) Tao, C.; Ruan, S.; Zhang, X.; Xie, G.; Shen, L.; Kong, X.; Dong, W.; Liu, C.; Chen, W. Performance Improvement of Inverted Polymer Solar Cells with Different Top Electrodes by Introducing a MoO3 Buffer Layer. *Appl. Phys. Lett.* **2008**, *93* (19), 193307.

(17) Gupta, S. K.; Sharma, A.; Banerjee, S.; Gahlot, R.; Aggarwal, N.; Deepak; Garg, A. Understanding the Role of Thickness and Morphology of the Constituent Layers on the Performance of Inverted Organic Solar Cells. *Sol. Energy Mater. Sol. Cells* **2013**, *116*, 135−143.

(18) Kim, J. S.; Park, J. H.; Lee, J. H.; Jo, J.; Kim, D.-Y.; Cho, K. Control of the Electrode Work Function and Active Layer Morphology Via Surface Modification of Indium Tin Oxide for High Efficiency Organic Photovoltaics. *Appl. Phys. Lett.* **2007**, *91*, 112111.

(19) Song, W.; So, S. K.; Wang, D.; Qiu, Y.; Cao, L. Angle Dependent X-Ray Photoemission Study on UV-Ozone Treatments of Indium Tin Oxide. *Appl. Surf. Sci.* **2001**, *177* (3), 158−164.

(20) Kim, J. S.; Granström, M.; Friend, R. H.; Johansson, N.; Salaneck, W. R.; Daik, R.; Feast, W. J.; Cacialli, F. Indium−Tin Oxide Treatments for Single- and Double-Layer Polymeric Light-Emitting Diodes: The Relation between the Anode Physical, Chemical, and Morphological Properties and the Device Performance. *J. Appl. Phys.* **1998**, *84* (12), 6859−6870.

(21) Khan, M. Z. H.; Nakanishi, T.; Osaka, T. Effects of Chemical Treatment of Indium Tin Oxide Electrode on Its Surface Roughness and Work Function. *Surf. Coat. Technol.* **2014**, *244* (0), 189−193.

(22) Chaney, J. A.; Koh, S. E.; Dulcey, C. S.; Pehrsson, P. E. Surface Chemistry of Carbon Removal from Indium Tin Oxide by Base and Plasma Treatment, with Implications on Hydroxyl Termination. *Appl. Surf. Sci.* **2003**, *218* (1−4), 259−267.

(23) You, Z. Z.; Dong, J. Y. Electrical and Optical Characteristics of Polymer Light-Emitting Devices with Surface-Treated Indium-Tin-Oxide Electrodes. *Microelectron. J.* **2007**, *38* (1), 108−113.

(24) Kim, J.-S.; Cacialli, F.; Friend, R. Surface Conditioning of Indium-Tin Oxide Anodes for Organic Light-Emitting Diodes. *Thin Solid Films* **2003**, *445* (2), 358−366.

(25) Clark, M. D.; Leever, B. J. Analysis of ITO Cleaning Protocol on Surface Properties and Polymer: Fullerene Bulk Heterojunction Solar

DOI: 10.1021/acsami.5b03583
ACS Appl. Mater. Interfaces 2015, 7, 16418−16427

Cell Performance. *Sol. Energy Mater. Sol. Cells* **2013**, *116* (0), 270−274.
(26) Chong, L.-W.; Lee, Y.-L.; Wen, T.-C. Surface Modification of Indium Tin Oxide Anodes by Self-Assembly Monolayers: Effects on Interfacial Morphology and Charge Injection in Organic Light-Emitting Diodes. *Thin Solid Films* **2007**, *515* (5), 2833−2841.
(27) Lai, T.-H.; Tsang, S.-W.; Manders, J. R.; Chen, S.; So, F. Properties of Interlayer for Organic Photovoltaics. *Mater. Today* **2013**, *16* (11), 424−432.
(28) Lee, T.-W.; Chung, Y. Control of the Surface Composition of a Conducting-Polymer Complex Film to Tune the Work Function. *Adv. Funct. Mater.* **2008**, *18* (15), 2246−2252.
(29) Yu, S.-Y.; Chang, J.-H.; Wang, P.-S.; Wu, C.-I.; Tao, Y.-T. Effect of ITO Surface Modification on the OLED Device Lifetime. *Langmuir* **2014**, *30* (25), 7369−7376.
(30) Hu, T.; Zhang, F.; Xu, Z.; Zhao, S.; Yue, X.; Yuan, G. Effect of UV−Ozone Treatment on ITO and Post-Annealing on the Performance of Organic Solar Cells. *Synth. Met.* **2009**, *159* (7−8), 754−756.
(31) Choi, J. K.; Jin, M. L.; An, C. J.; Kim, D. W.; Jung, H.-T. High-Performance of PEDOT/PSS Free Organic Solar Cells on an Air-Plasma-Treated Ito Substrate. *ACS Appl. Mater. Interfaces* **2014**, *6* (14), 11047−11053.
(32) Cheng, Y.-T.; Ho, J.-J.; Wang, C.-K.; Lee, W.; Lu, C.-C.; Yau, B.-S.; Nain, J.-L.; Chang, S.-H.; Chang, C.-C.; Wang, K. L. Improvement of Organic Solar Cells by Flexible Substrate and ITO Surface Treatments. *Appl. Surf. Sci.* **2010**, *256* (24), 7606−7611.
(33) Dong, W. J.; Jung, G. H.; Kim, S. Y.; Lee, J.-L. Effect of Ultraviolet−Ozone on ITO/P3HT Interface for PEDOT:PSS Free Polymer Solar Cells. *Sol. Energy Mater. Sol. Cells* **2013**, *109* (0), 240−245.
(34) Cho, J. M.; Kwak, S.-W.; Aqoma, H.; Kim, J. W.; Shin, W. S.; Moon, S.-J.; Jang, S.-Y.; Jo, J. Effects of Ultraviolet−Ozone Treatment on Organic-Stabilized ZnO Nanoparticle-Based Electron Transporting Layers in Inverted Polymer Solar Cells. *Org. Electron.* **2014**, *15* (9), 1942−1950.
(35) Sun, K.; Ouyang, J. Polymer Solar Cells Using Chlorinated Indium Tin Oxide Electrodes with High Work Function as the Anode. *Sol. Energy Mater. Sol. Cells* **2012**, *96* (0), 238−243.
(36) Udum, Y.; Denk, P.; Adam, G.; Apaydin, D. H.; Nevosad, A.; Teichert, C.; S. White, M.; S. Sariciftci, N.; Scharber, M. C. Inverted Bulk-Heterojunction Solar Cell with Cross-Linked Hole-Blocking Layer. *Org. Electron.* **2014**, *15* (5), 997−1001.
(37) Zhou, H.; Zhang, Y.; Seifter, J.; Collins, S. D.; Luo, C.; Bazan, G. C.; Nguyen, T.-Q.; Heeger, A. J. High-Efficiency Polymer Solar Cells Enhanced by Solvent Treatment. *Adv. Mater. (Weinheim, Ger.)* **2013**, *25* (11), 1646−1652.
(38) Zhang, K.; Hu, Z.; Duan, C.; Ying, L.; Huang, F.; Cao, Y. The Effect of Methanol Treatment on the Performance of Polymer Solar Cells. *Nanotechnology* **2013**, *24* (48), 484003.
(39) Alemu, D.; Wei, H.-Y.; Ho, K.-C.; Chu, C.-W. Highly Conductive PEDOT:PSS Electrode by Simple Film Treatment with Methanol for ITO-Free Polymer Solar Cells. *Energy Environ. Sci.* **2012**, *5* (11), 9662−9671.
(40) Ye, L.; Jing, Y.; Guo, X.; Sun, H.; Zhang, S.; Zhang, M.; Huo, L.; Hou, J. Remove the Residual Additives toward Enhanced Efficiency with Higher Reproducibility in Polymer Solar Cells. *J. Phys. Chem. C* **2013**, *117* (29), 14920−14928.
(41) Cheun, H.; Fuentes-Hernandez, C.; Zhou, Y.; Potscavage, W. J.; Kim, S.-J.; Shim, J.; Dindar, A.; Kippelen, B. Electrical and Optical Properties of ZnO Processed by Atomic Layer Deposition in Inverted Polymer Solar Cells. *J. Phys. Chem. C* **2010**, *114* (48), 20713−20718.
(42) Liang, Z.; Zhang, Q.; Wiranwetchayan, O.; Xi, J.; Yang, Z.; Park, K.; Li, C.; Cao, G. Effects of the Morphology of a ZnO Buffer Layer on the Photovoltaic Performance of Inverted Polymer Solar Cells. *Adv. Funct. Mater.* **2012**, *22* (10), 2194−2201.
(43) Tang, W. M.; Greiner, M. T.; Lu, Z. H.; Ng, W. T.; Nam, H. G. Effects of UV-Ozone Treatment on Radio-Frequency Magnetron Sputtered ZnO Thin Films. *Thin Solid Films* **2011**, *520* (1), 569−573.
(44) Lim, F. J.; Set, Y. T.; Krishnamoorthy, A.; Ouyang, J.; Luther, J.; Ho, G. W. Addressing the Light-Soaking Issue in Inverted Organic Solar Cells Using Chemical Bath Deposited Fluorinated Tiox Electron Transport Layer. *J. Mater. Chem. A* **2015**, *3* (1), 314−322.
(45) Zhang, K.; Hu, Z.; Duan, C.; Ying, L.; Huang, F.; Cao, Y. The Effect of Methanol Treatment on the Performance of Polymer Solar Cells. *Nanotechnology* **2013**, *24* (48), 484003.
(46) Lee, S. J.; Kim, H. P.; Yusoff, A. R. b. M.; Jang, J. Understanding the Role of Organic Polar Solvent Induced Nanoscale Morphology and Electrical Evolutions of P3HT:PCBM Composite Film. *Org. Electron.* **2015**, *25*, 50−56.
(47) Nonnenmacher, M.; O'Boyle, M. P.; Wickramasinghe, H. K. Kelvin Probe Force Microscopy. *Appl. Phys. Lett.* **1991**, *58* (25), 2921−2923.
(48) Nam, S.; Jang, J.; Cha, H.; Hwang, J.; An, T. K.; Park, S.; Park, C. E. Effects of Direct Solvent Exposure on the Nanoscale Morphologies and Electrical Characteristics of PCBM-Based Transistors and Photovoltaics. *J. Mater. Chem.* **2012**, *22* (12), 5543−5549.
(49) Mallajosyula, A. T.; Sundar Kumar Iyer, S.; Mazhari, B. Charge Transport in Polythiophene:Fullerene:Nanotube Bulk Heterojunction Photovoltaic Devices Investigated by Impedance Spectroscopy. *Curr. Appl. Phys.* **2013**, *13* (4), 677−683.
(50) Zhang, Y.; Li, L.; Yuan, S.; Li, G.; Zhang, W. Electrical Properties of the Interfaces in Bulk Heterojunction Organic Solar Cells Investigated by Electrochemical Impedance Spectroscopy. *Electrochim. Acta* **2013**, *109* (0), 221−225.
(51) Yao, E.-P.; Chen, C.-C.; Gao, J.; Liu, Y.; Chen, Q.; Cai, M.; Hsu, W.-C.; Hong, Z.; Li, G.; Yang, Y. The Study of Solvent Additive Effects in Efficient Polymer Photovoltaics Via Impedance Spectroscopy. *Sol. Energy Mater. Sol. Cells* **2014**, *130* (0), 20−26.
(52) Zhang, Y.; Yuan, S.; Li, Y.; Zhang, W. Enhanced Electron Collection in Inverted Organic Solar Cells Using Titanium Oxide/Reduced Graphene Oxide Composite Films as Electron Collecting Layers. *Electrochim. Acta* **2014**, *117*, 438−442.
(53) Garcia-Belmonte, G.; Munar, A.; Barea, E. M.; Bisquert, J.; Ugarte, I.; Pacios, R. Charge Carrier Mobility and Lifetime of Organic Bulk Heterojunctions Analyzed by Impedance Spectroscopy. *Org. Electron.* **2008**, *9* (5), 847−851.
(54) Leever, B. J.; Bailey, C. A.; Marks, T. J.; Hersam, M. C.; Durstock, M. F. In Situ Characterization of Lifetime and Morphology in Operating Bulk Heterojunction Organic Photovoltaic Devices by Impedance Spectroscopy. *Adv. Energy Mater.* **2012**, *2* (1), 120−128.
(55) Liu, Y.-X.; Lü, Y.; Ning, Y.; Lu, Y.-Z.; Lu, Q.-P.; Zhang, C.-M.; Fang, Y.; Tang, A.-W.; Hu, Y.-F.; Lou, Z.-D.; et al. Effects of Acetone-Soaking Treatment on the Performance of Polymer Solar Cells Based on P3HT.PCBM Bulk Heterojunction. *Chin. Phys. B* **2014**, *23* (11), 118802.
(56) Guo, S.; Cao, B.; Wang, W.; Moulin, J.-F. o.; Muller-Buschbaum, P. Effect of Alcohol Treatment on the Performance of PTB7:PC71BM Bulk Heterojunction Solar Cells. *ACS Appl. Mater. Interfaces* **2015**, *7* (8), 4641−4649.

DOI: 10.1021/acsami.5b03583
ACS Appl. Mater. Interfaces 2015, 7, 16418−16427